Journal of Materials Science: Materials in Medicine (2018) 29:189
https://doi.org/10.1007/s10856-018-6197-3

BIOCOMPATIBILITY STUDIES

Original Research

The comparison of biocompatibility and osteoinductivity between multi-walled and single-walled carbon nanotube/PHBV composites

Weiyi Pan[1] · Xun Xiao[1] · Jinle Li[1] · Shibing Deng[1] · Qin Shan[1] · Yuan Yue[1] · Ye Tian[1] · Neel R Nabar[2] · Min Wang[1] · Liang Hao[1]

Received: 8 July 2018 / Accepted: 25 November 2018 / Published online: 10 December 2018

Abstract

The applications of poly (3-hydroxybutyrate-co-3-hydroxyvalerate) (PHBV) in tissue engineering have been widely studied. This study aimed to compare the biocompatibility and osteoinductivity of single-walled carbon nanotubes (SWCNTs)/PHBV composites with multi-walled CNTs (MWCNTs)/PHBV composites. CNTs were dispersed in PHBV by ultrasonication and composites were created using thermal injection moulding. In order to test their biocompatibility and osteoinductivity. Rat osteoblasts (rOBs) were then cultured and seeded on the composites. The composites were implanted in rat femoral bone defects. Our results showed that lower weight percentages of SWCNTs and MWCNTs (2–4%) improved both their mechanical and thermal decomposition properties. However, further reduction of rOBs cell death was observed in MWCNTs/PHBV. SWCNTs were shown to upregulate the expression of *Runx-2* and *Bmp-2* in early stage significantly, while MWCNTs showed a stronger long-term effect on *Opn* and *Ocn*. The in vivo result was that MWCNTs/PHBV composites induced intact rounding new bone, increased integration with new bone, and earlier completed bone remodeling when compared with SWCNTs. Immunohistochemistry also detected higher expression of RUNX-2 around MWCNTs/PHBV composites. In conclusion, there were no differences observed between SWCNTs and MWCNTs in the reinforcement of PHBV, while MWCNTs/PHBV composites showed better biocompatibility and osteoinductivity both in vitro and in vivo.

Supplementary information The online version of this article (https://doi.org/10.1007/s10856-018-6197-3) contains supplementary material, which is available to authorized users.

✉ Liang Hao
hxkqhl@foxmail.com

[1] The State Key Laboratory of Oral Diseases & National Clinical Research Centre for Oral Diseases, Department of Prosthodontics, West China Hospital of Stomatology, Sichuan University, Sichuan, People's Republic of China

[2] Sidney Kimmel Medical College at Thomas Jefferson University, Philadelphia, PA, USA

Graphical Abstract

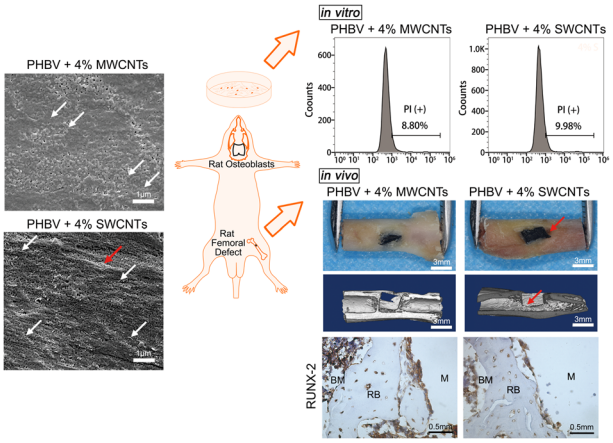

1 Introduction

Poly (3-hydroxybutyrate-*co*-3-hydroxyvalerate) (PHBV) is a member the of polyhydroxyalkanoate (PHA) chemical family, which was first manufactured and commercialized as "Biopol" in 1983 [1]. PHBV can be synthesized by bacterial-like *Ralstonia eutropha* and *Paracoccus denitrificans* as energy storage compounds under limited growth conditions [2]. Members of the PHA family possess common properties like good biodegradability and biocompatibility. Biocompatibility of PHAs with bone and cartilage has been demonstrated by previous in vivo and in vitro experiments [3, 4]. Hence, PHBV has been well investigated in its application to bone substitutes, vascular grafts, and drug carriers [5–8]. However, the hydrophobicity of PHAs might affect the initial adhesion and growth of host cells [9]. Short chain length PHAs are rigid but brittle, and medium chain length PHAs are elastomeric but lack mechanical properties [10]. Also, PHBV is thermoplastic and can be shaped by thermal injection molding, while its poor thermostability increases difficulty in processing [11].

Since their discovery in 1991, carbon nanotubes (CNTs) have gained attention due to their characteristic helical structure and properties [12]. CNTs can be categorized according to the number of layers: single-walled CNTs (SWCNTs), double-walled CNTs (DWCNTs), and multi-walled CNTs (MWCNTs). CNTs possess several remarkable properties, including thermal and electronic conductivity [13, 14] and high modulus of elasticity and tensile strength [15, 16], among others. The application of CNTs is mainly focused on the fields of tissue engineering and drug delivery. CNTs have been proven to be biocompatible with osteoblasts [17, 18], cardiac myocytes [19, 20] and neurons [21]. Furthermore, melding CNTs into biopolymer material can improve their mechanical properties [22–24].

According to the character of PHBV and CNTs outlined above, the addition of CNTs into PHBV might improve its properties. It has been previously reported that the addition of MWCNTs into poly(3-hydroxybutyrate), another member of PHA family, showed improvement in surface properties, electrical resistance and OBs proliferation [25, 26]. Our previous work showed that, when compared with pure PHBV, MWCNTs/PHBV composites had improved mechanical properties, better biocompatibility both in vitro and in vivo [27]. However, no study has compared MWCNTs with SWCNTs for application in bone tissue engineering. Thus, in this study, we aimed to compare MWCNTs/PHBV and SWCNTs/PHBV composites and the determination of optimum weight percentage (wt%) of CNTs in these composites. According to our results, there were no differences between SWCNTs/PHBV and MWCNTs/PHBV in terms of mechanical properties and thermostabilities, while MWCNTs/PHBV showed better biocompatibility and osteoinductivity. Importantly, 4% proved to be the optimum wt% of MWCNTs in composites to balance mechanical properties and biocompatibility.

2 Materials and methods

2.1 Fabrication of PHBV/CNTs composites

2.1.1 Homogenization of CNTs and PHBV

PHBV powder (>98% purity, 100% chiral) was purchased from TianAn Biologic Materials Co. Ltd. (Zhejiang, China). Carboxyl group functionalized MWCNTs (purity: >98%; -COOH content: 1.23 wt%; outer diameter: 20–30 nm; length: 10–30 μm) and SWCNTs (purity: >95%; oxygen content: >9 wt% outer diameter: 1–2 nm; length: 5–30um) were purchased from Chengdu Organic Chemicals Co. Ltd. (Sichuan, China). The PHBV/CNTs composites were

fabricated as previously described [27]. Briefly, CNTs were dispersed with 6 h magnetic stirring and 15 min ultrasonic in chloroform. An ultrasonic cell homogenizer (JY92-IIDN), purchased form Ningbo Scientz Biotechnology Co. Ltd. (Zhejiang, China) was used, and parameters were set as follows: Φ6 ultrasonic probe (1/4″, 60–650 W), working time 2 s, interval time 2 s, 25% maximum power. Then, PHBV powder was added to the mixture followed by a 15 min ultrasonic dispersion. After dispersion, chloroform was removed by a rotatory evaporator and the composites were dried until there was no weight change. The composites were grouped by weight percentage (0%, 0.5%, 1%, 2%, 4%, 8%) of MWCNTs or SWCNTs.

2.1.2 Injection molding of composites

The composites were molded as cuboids (80 mm × 10 mm × 4 mm) and disks (diameter = 20 mm, thickness = 2 mm) using a thermal injection molding machine (Thermo Scientific HAAKE™ MiniJet pro, MA USA). The cylinder temperature was set to 180 °C, and the mold temperature was set at 60 °C. The injection pressure was set to 600 bar for 6 s and maintained at 200 bar for 2 s.

2.2 Characterization of PHBV/CNTs composites

2.2.1 Scanning electron microscopy (SEM)

The inner morphology of the composites was observed by SEM (FEI, Inspect F; MA USA) to see the effect of ultrasonic depression. Cuboid composites were first sectioned and the fracture surfaces were ground and polished. Then the composites were mounted on a stub and coated with gold. The images were captured at an acceleration voltage of 5 kV.

2.2.2 Mechanical properties

The flexural strength of composites was tested by a universal mechanical testing machine (Instron, 4302; MA USA) according to standard test methods obtained from the American Society for Testing and Materials (ASTM D790). The support span was set at 64 mm, and the rate of crosshead motion was set at 0.5 mm/min. Additionally, the temperature was maintained at 23 °C for all tests. Five samples were tested in each group, and mean maximum flexural stress was recorded as the flexural strength for that composite (MPa).

2.2.3 NaNNaNThermal decomposition properties

A thermal gravimetric analyzer (TA Instruments Q600, DE USA) was used to test the thermostability of composites. The heating rate was set at 10 °C/min (room temperature to 500 °C) temperature range; an inert atmosphere was maintained with a continuous nitrogen flow (30 ml/min). The thermal decomposition temperature (T_0) was defined as the temperature at which the material quality decreases 5%.

2.2.4 NaNNaNX-ray diffraction (XRD)

An x-ray diffractometer (Rigaku, UltimaIV; Tokyo Japan) was used to characterize the crystal lattice by detecting the intensity of the diffracted beam at different angles. The scan range (2θ) was 5–100° with Cu used as a radiation source; the scanning speed was set at 1°/min.

2.2.5 NaNNaNFourier transform infrared spectroscopy (FTIR)

Fourier transform infrared spectrometer (Thermo Scientific, NicoIet380; MA USA) was used to obtain an infrared spectrum of absorption caused by vibration of different functional groups. This provided information about the composition of the composites. Samples were then finely polished with sandpaper in order. The scanning range of the infrared spectrum was 4000–600 cm^{-1}, and the resolution was 4 cm^{-1}. In total, 1869 scans were performed on each sample.

2.3 In vitro biocompatibility and osteoinductivity

2.3.1 Primary culture of rat osteoblasts (rOBs)

Newborn Sprague Dawley (SD) rats (<three days-old) were purchased from the laboratory animal center of Sichuan University and sacrificed to obtain primary osteoblasts. Briefly, the cranium of two rats was dissected and washed in phosphate buffered solution (PBS) and a penicillin (1000U/ml)-streptomycin (1 mg/ml) solution (Hyclone; UT USA). Then, the cranium was sheared into pieces and incubated with 0.25% trypsin for 15 min and collagenase II (1 mg/ml, Gibco; CA USA) for 1 h at 37 °C. After centrifugation (1,000 rpm, 5 min) and discarding the collagenase solution, the precipitate was resuspended by low glucose type Dulbecco's modified eagle medium (DMEM, Hyclone; UT USA) containing 10% fetal bovine serum (Corning; NY USA) and seeded into a petri dish. After culturing at 37 °C in 5% CO_2 for 5 days, cranium pieces were washed with PBS and the culture medium was changed. The adherent cells were used for further testing or passed when they were 70–80% confluent.

2.3.2 Cell viability testing by Cell Counting Kit-8 (CCK-8)

Disk-like composites were trimmed to fit 96-well plates. After ultraviolet and ozone disinfection (Kenge Wang

Ozone Electrical Equipment; Sichuan China), rOBs were seeded directly onto composites. Cell viability was measured 1, 3, 5, 7 days after cell seeding by CCK-8 (Dojindo; Kumamoto Japan) according to the manufacturer's instruction. The absorbance at 450 nm was measured by a microplate reader (Thermo Scientific, Varioskan™ Flash; MA USA). Cells seeded directly into culture plate were used as the control group. The absorbance of each group was standardized according to the control group at each time point.

2.3.3 Cell death analysis via flow cytometry

The disk-like composites were trimmed to fit into 6-well plates and rOBs were seeded after disinfection. Cells were harvested by centrifugation at 2000 rpm for 5 min and then rinsing twice with PBS. Cells were then resuspended directly in propidium iodide (PI, KeyGEN Bioteck; Jiangsu China) staining solution (8 μM) and incubated at room temperature for 45 min away from light. Stained cells were then tested by flow cytometer (Beckman Coulter, Cytomics™ FC 500; CA USA) using optical filters for PI (>600 nm). The percentage of PI-positive cells from each treatment group was analyzed by FlowJo v10.0.7r2 (OR USA).

2.3.4 RNA extraction and qPCR

Total RNA was extracted using MiniBEST Universal RNA Extraction Kit (Takara Bio; Shiga Japan), and the reverse transcription of mRNA was conducted using RevertAid First Strand cDNA Synthesis Kit (Thermo Scientific, MA USA), according to the manufacturer's instructions. qRT-PCR cas carried out using SYBR® Premix Ex TaqTM II (Takara Bio; Shiga Japan) on a BioRad CFX96 thermocycler (CA, USA). The following primers were purchased from TsingKe Biological Technology (Beijing China): *Runx-2* (forward: TCTTCCCAAAGCCAGAGCG, reverse: TGCCATTCGAGGTGGTCG); *Bmp-2* (forward: TGGGTT TGTGGTGGAAGTGGC, reverse: TGGATGTCCTTTAC CGTCGTG); *Opn* (forward: CCAAGCGTGGAAACA-CACAGCC, reverse: GGCTTTGGAACTCGCCTGACT G); *Ocn* (forward: GCCCTGACTGCATTCTGCCTCT, reverse: TCACCACCTTACTGCCCTCCTG). Housekeeping gene *Actb* (forward: CACCCGCGAGTA-CAACCTTC, reverse: CCCATACCCACCATCACACC) was used as an endogenous control.

2.4 In vivo biocompatibility and osteoinductivity

2.4.1 Animal feeding

The animal experimentation included in this study was approved by the Sichuan University Animal Review Committee. Male SD rats (7- to 8-week-old, approximately 250 g) were purchased from Dashuo Biotechnology (Sichuan, China) and maintained in the animal facility of State Key Laboratory of Oral Disease at Sichuan University. The animals were fed a conventional diet *ad libitum* and illumination was provided according to conventional circadian rhythm (12-hour light/dark cycle). Five rats were allocated to each group and all animal experimentation was repeated three times ($n = 15$ per group in total).

2.4.2 Implantation of composite and sample collection

After adaption for one week, composites were implanted in rat femurs under general anesthesia with 10% chloral hydrate (3 ml/kg intraperitoneally). A 3.5 mm × 2.5 mm defect close to epiphysis was drilled with a round bur intermittently at low speed with physiological saline cooling. After a fitted composite cuboid was knocked into the bone defect, the wound was sutured tightly. Ampicillin (Solarbio Life Sciences; Beijing China) was injected intramuscularly (250 mg/ml, 0.5 ml/d) for 3d postoperatively to prevent infection. Groups of rats were sacrificed at 5 and 10 weeks after the operation via overdose anesthetics. Femurs were harvested and fixed in 4% paraformaldehyde for 24 h, washed with tap water and preserved in 70% ethanol.

2.4.3 Micro CT analysis

Femur samples were steadied with plastic foam in the sample holder. Scanning was performed every 20 μm at medium resolution using vivaCT80 (SCANCO Medical; Zurich Switzerland). After scanning, cross-sectional slices were reconstructed, on which the region of interest (ROI) was defined around the newly formed bone near composites. ROI, relative bone volume (bone volume/total volume, BV/TV), connectivity density ($1/mm^3$), structure model index (0–3; 0 for parallel plates, 3 for cylindrical rods), trabecular morphology parameters (number: 1/mm, thickness: mm, separation: mm) were measured. A 3D reconstruction was performed using Mimics Research v19.0.0 (Materialise; Leuven Belgium).

2.4.4 Histological analysis by hard tissue slices

Fixed samples were gradient dehydrated with ethanol (75%, 80%, 85%, 90%, 95%, 100%; 24 h for each) and cleared with xylene for 4 h. Then, undecalcified tissue was infiltrated and embedded with methyl-methacrylate and polymerized at 4 °C for 5d. After complete polymerization, slices were cut perpendicular to the long-axis of the femur at a thickness of 800 μm using a hard tissue slicer (Bowen Lab, 08–2; Shanxi China). After methylene blue and acid

fuchsin staining, the slices were mounted and observed with an optical microscope (Leica, Hesse-Darmstadt Germany).

2.4.5 Immunohistochemistry (IHC)

Samples were decalcified in 10% ethylenediaminetetraacetic acid (EDTA) (with 0.01 M Tris-HCl buffer, pH = 7.0) for 30d at room temperature, then dehydrated, immersed in paraffin wax, and sectioned (6 μm). rabbit anti-rat RUNX-2 antibody (1:500; Cell Signaling Technology; MA USA) was used to observe the expression and location of the target protein in the sections. Relative quantitative analysis, namely comparing the integral optical density (IOD) of the positive area, was performed using Image-Pro Plus v6.0.0 (Media Cybernetics; MD USA).

2.5 Statistical analysis

All data were reported as means ± standard deviation (SD). P value < 0.05 was considered statistically significant. For mean comparisons between multiple groups, one-way analysis of variance (ANOVA) was used, and Tukey's honestly significant difference test was used for multiple comparisons. All the statistical analyses and generation of statistical graphs were performed using PRISM v6.0c (GraphPad; CA USA).

3 Results

3.1 Characterization of PHBV/CNTs composites

One of the major applications of CNTs in tissue engineering is as a nano-filler to strengthen the mechanical properties of composites. A precondition of this application is less agglomeration, namely the complete dispersion of CNTs in composites. By performing SEM scanning, we observed that CNTs could be dispersed in PHBV by ultrasound when the weight percentage (wt%) of CNTs was low (Fig. 1a, white arrow). Sporadic small agglomeration was observed by SEM with up to 2 wt% of added MWCNTs and 4% added SWCNTs (Fig. 1a, red arrow). This indicated that the complete dispersion of SWCNTs was easier to achieve. However, when the wt% of CNTs was increased to 8%, large agglomerations could be observed both in MWCNT group and SWCNT group.

Next, we tested the flexural strength of composites. Even adding a small amount of CNTs (0.5 wt%) could significantly strengthen the mechanical properties of the composites compared with pure PHBV ($P < 0.001$) (Fig. 1b). However, the flexural strength decreased if the wt% of CNTs was too high. A similar fluctuation in flexural strength was observed among MWCNTs and SWCNTs ($P > 0.05$), which indicated that 4% was the optimal wt% for CNTs in composites (Fig. 1c). In order to achieve the optimal mechanical properties of PHBV, we chose to use thermal injection molding for fabrication of the composites. Since the melting temperature of PHBV was close to its decomposition temperature, thermal gravimetric analysis was performed to determine whether the addition of CNTs could improve the thermal decomposition property of PHBV. Our data showed that the addition of more than 4% of both MWCNTs and SWCNTs would increase the decomposition temperature of the composites, while low wt % might cause an adverse effect (Fig. 1d).

The mechanism of CNTs effect on composite properties was explored by performing XRD to determine the crystallization pattern of PHBV. Our result showed that the location of main diffraction peaks of PHBV did not change when CNTs was added (Appendix Figs. 1 and 2). However, the intensity of the peaks around 13.6° and 17.0° initially rose then deceased along with the addition of CNTs, while the intensity of the peaks around 22.4° showed the opposite pattern. The change of intensity of diffraction peaks indicated the change in the arrangement of PHBV crystal lattice, which might explain the mechanism by which CNTs reinforces the composites.

3.2 In vitro biocompatibility

One of the essential conditions of the application of macromolecular materials in bone tissue engineering is biocompatibility. Functionalization is the most common method to improve the hydrophobicity of CNTs. Hence, we assumed that the addition of –COOH functionalized CNTs (f-CNTs) might enhance the hydrophobicity of PHBV as well, thus improving the biocompatibility of the composites. First, the infrared spectrum of different groups of composites was obtained to identify their functional groups (Appendix Figs. 3 and 4). The intensity of absorption peak at 3438 cm^{-1}, representing the –OH group in carboxyl group of f-CNTs, increased with the addition of f-CNTs, indicating that the functional group was not lost during the fabrication of the composites.

CCK-8 is an indirect way to measure cell viability by detecting the enzymatic activity of dehydrogenases, which reflects the biocompatibility of the composites. Two and four wt% of MWCNTs and SWCNTs group (2%/4%-M/S), respectively, were chosen for further testing according to the dispersion of CNTs, mechanical properties and thermal stability. When compared with the control group, the cell viability of rOBs showed different levels of inhibition 1d after seeding on the composites, which aggravated on 3d (Fig. 2a). Interestingly, cell viability was increased in all groups on 5d. When the testing time was prolonged to 7d, cell viability in all groups recovered to the level observed

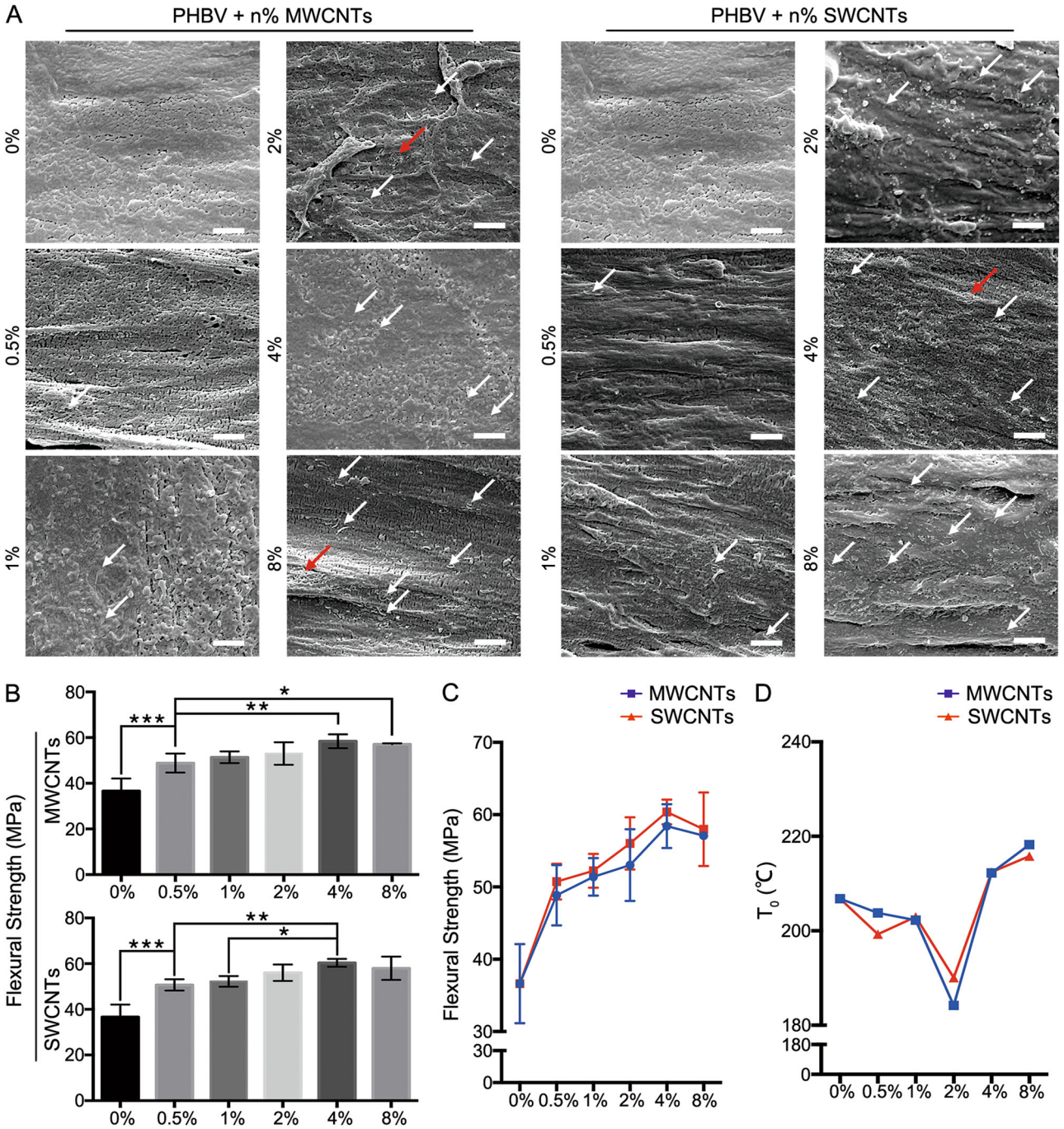

Fig. 1 Uniformly blending of MWCNTs and SWCNTs both strengthen the mechanical and thermal properties of PHBV. **a** The inner morphology of composites was obtained by SEM. Most of the CNTs were completely dispersed (white arrow), while small aggregation (red arrow) occurred when the wt% of CNTs increased. **b** Flexural strength observed by three-point bending test ($n = 5$). Improvement to the mechanical property of the composites could be observed with the addition of CNTs. **c** A comparison of mechanical properties between MWCNTs and SWCNTs composites represented as the combined line graph; no significant differences were observed. **d** The thermal decomposition temperature (T_0) of a different group of composites. $^*P < 0.05$; $^{**}P < 0.01$; $^{***}P < 0.001$. Scale bar: 1 μm

1d after seeding. However, no statistically significant difference was found between the different groups.

Since CCK-8 only gives a side reflection of cell proliferation, we further performed flow cytometry to detect dead cells. The loss of cytomembrane integrity gives permission for entry of PI and staining of the cell nucleus. Thus, PI positive cells were identified as dead cells. Remarkably, 12% of cells were identified as dead cells 1d after seeding onto pure PHBV, while the addition of CNTs decreased the percentage of dead cells (Fig. 2b).

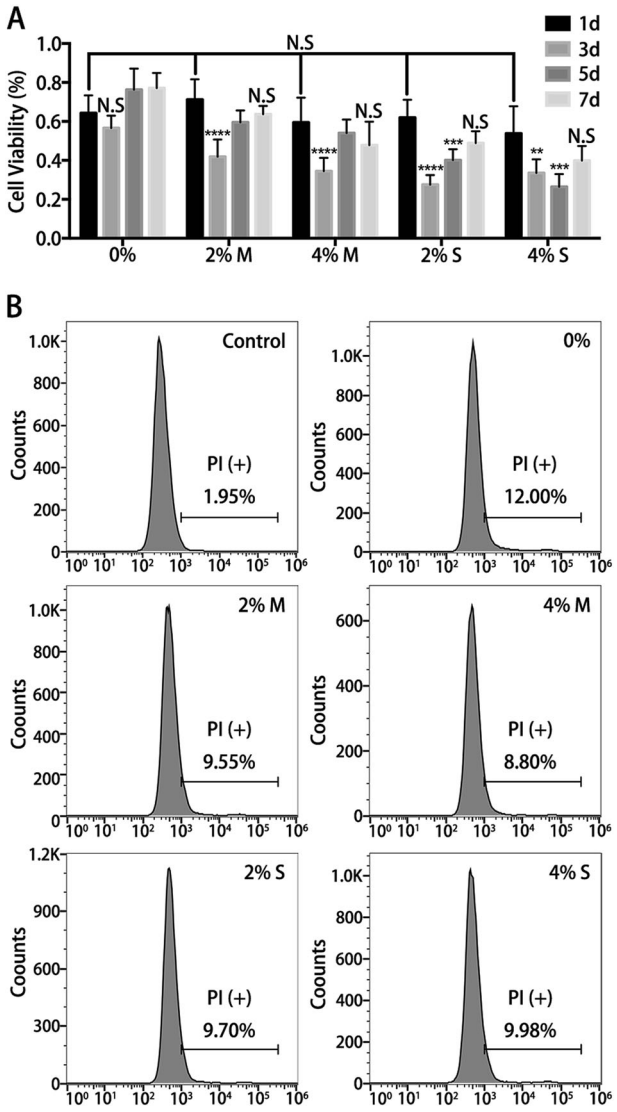

Fig. 2 MWCNTs/PHBV composites showed better biocompatibility in vitro. **a** The cell viability percentage of rat osteoblasts 1, 3, 5, 7 days after seeding. Data were calculated from the absorbance obtained by CCK-8 ($n = 5$) and standardized according to the control group. Rat osteoblasts seeded directly into a culture plate was considered to be the control group, of which the column was omitted. The complete data are shown in Appendix Fig. 5.**b** The percentage of PI-positive cells (dead cells) obtained by flow cytometry. *$P < 0.05$; **$P < 0.01$; ***$P < 0.001$; ****$P < 0.0001$; N.S not significant. All testing was replicated three times

Specifically, 4% MWCNTs group decreased the PI-positive cells ratio to 8.8%, which indicate the improvement of biocompatibility by addition of f-CNTs.

3.3 In vitro osteoinductivity

Another characteristic of bone tissue engineering materials is osteoinductivity, the ability to induce new bone formation. This induction can be observed via the expression level of the osteogenesis-related genes in vitro. We thus performed qRT-PCR to detect the mRNA level of *Runx-2*, *Bmp-2*, *Opn* and *Ocn*. All the four genes showed a high expression level in the pure PHBV group and composites groups when compared with the control group (direct seeding onto a cell culture plate) at 1d after seeding (Fig. 3). Specifically, seeding on 4% SWCNTs/PHBV composites resulted in a 3.73-fold expression of *Runx-2* and 6.68-fold expression of *Bmp-2*, which higher than pure PHBV and MWCNTs/PHBV composites ($P < 0.01$). However, the mRNA level of the other two genes did not show significant increase at day 3, which corresponded to a change in cell viability measured by CCK-8. Interestingly, when we prolonged the incubation time to 7 days, two late-stage marker genes, *Opn* and *Ocn*, had a significantly higher expression level in the 4% MWCNTs/PHBV composite group when compared to pure PHBV and SWCNTs/PHBV composites groups ($P < 0.01$). No significant differences were found in the mRNA level of *Runx-2* and *Bmp-2* between several composites groups. When comparing 2% and 4% of CNTs in composites, the 4% group demonstrated superior mechanical properties, thermal stability, and osteoinductivity. We thus chose this composite for further experimentation.

3.4 In vivo biocompatibility and osteoinductivity

Since we had previously observed that the addition of f-CNTs improved the biocompatibility and osteoinductivity of composites, further animal experiments were designed to observe the interface reaction between material and host tissue in vivo. More new bone formation covering the composite (Fig. 4a, white dashed area) and regenerated trabeculae (Fig. 4a, white arrow with black outline) could be observed in the rats treated with 4% MWCNTs/PHBV 5 weeks after implantation. Unlike 4% MWCNTs group, some connective tissue and region without new bone formation could be observed at the interface in pure PHBV and 4% SWCNTs groups (Fig. 4a, red arrow). Finally, 10 weeks after implantation, similar intact and new regenerated compact bone could be observed surrounding the composites from all the three groups, while the new bone covering the material (Fig. 4a, white dashed area) could be observed only in the 4% MWCNTs group rather than in the pure PHBV and 4% SWCNTs groups.

We further performed quantitative analysis with microCT results. Five weeks after implantation, BV/TV was significantly higher in the 4% MWCNTs group when compared with pure PHBV and 4% SWCNTs groups ($P < 0.05$) (Fig. 4b). Several parameters also indicated that the 4% MWCNTs group gained more newly formed trabecular and had less separation with more connection between trabecula. Similar to the above result, no significant

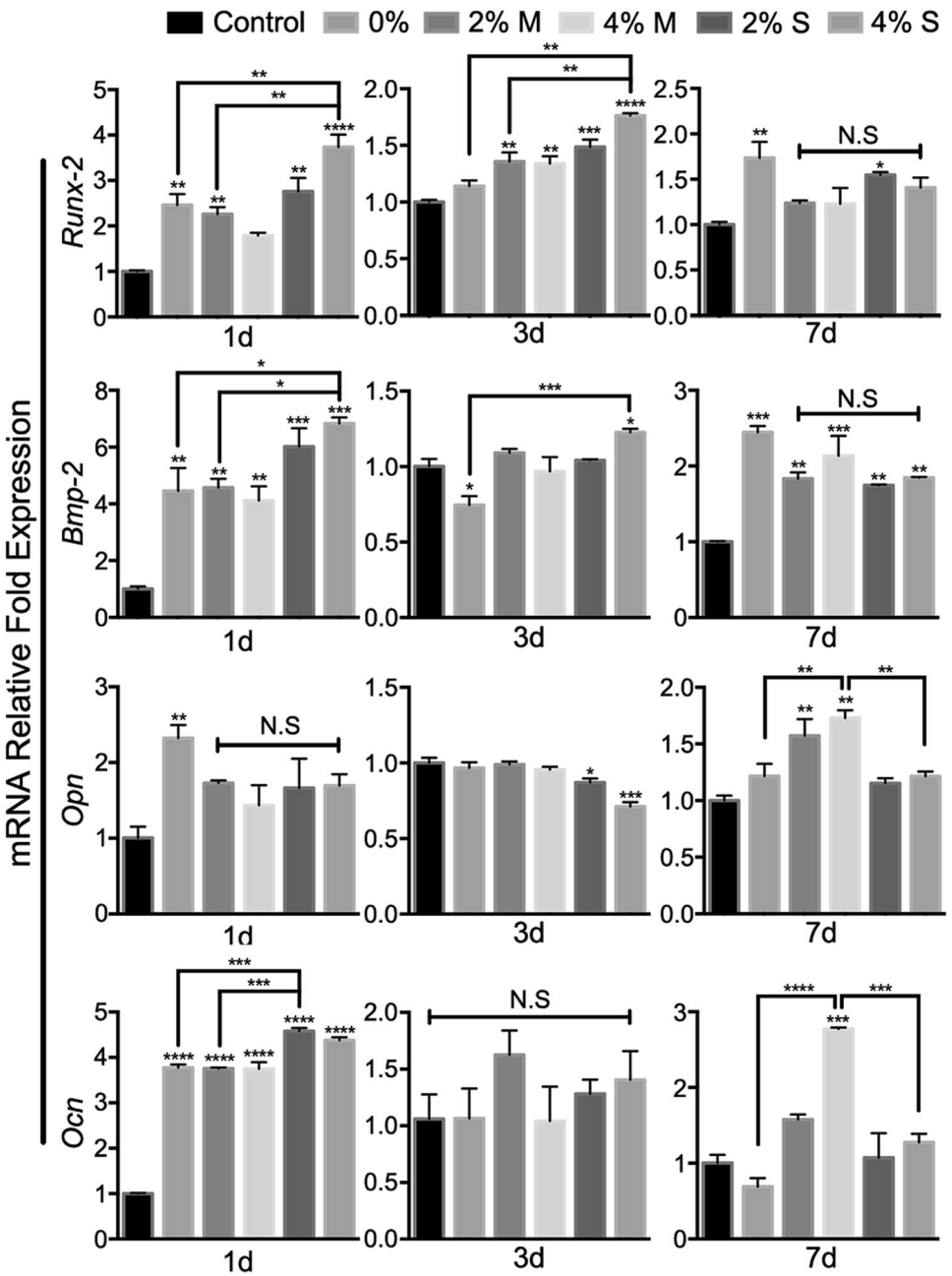

Fig. 3 SWCNTs demonstrated better short-term effect and MWCNTs demonstrated better long-term effect on the osteoinductivity of the composites. The relative expression of rat osteoblasts mRNA of osteogenic-related genes obtained by qRT-PCR at different time points after seeding of the composites ($n = 3$). *Actb* was used as an endogenous control. $^{*}P < 0.05$; $^{**}P < 0.01$; $^{***}P < 0.001$; $^{****}P < 0.0001$; N.S not significant. All testing was replicated three times

difference was found between three groups 10 weeks after implantation.

Newly regenerated bone was stained as dark red and could be observed directly through hard tissue slices (Fig. 5a). Almost all the interface between composite and bone marrow was covered with new bone in the 4% MWCNTs group 5 weeks after implantation. However, some fiber-like tissues could be observed between PHBV (0% group) and new bone (red arrow), and absence of new bone could be observed in some areas of the interface in 2% SWCNTs group (white arrow). Ten weeks after implantation, intact rounding bone and newly formed bone trabecula, apparent bone remodeling, could be observed in the PHBV and 4% MWCNTs groups.

In the end, IHC was performed to determine whether the induction of osteogenesis-related protein expression could be observed in vivo. Strong expression of RUNX-2 located in the cell nucleus was detected in the osteocytes of regenerated bone and bone marrow cells five weeks after composite implantation in the 4% MWCNTs group (Fig. 5B). The IOD quantification also showed a similar result, supporting the conclusion that 4% MWCNTs/PHBV composite had stronger

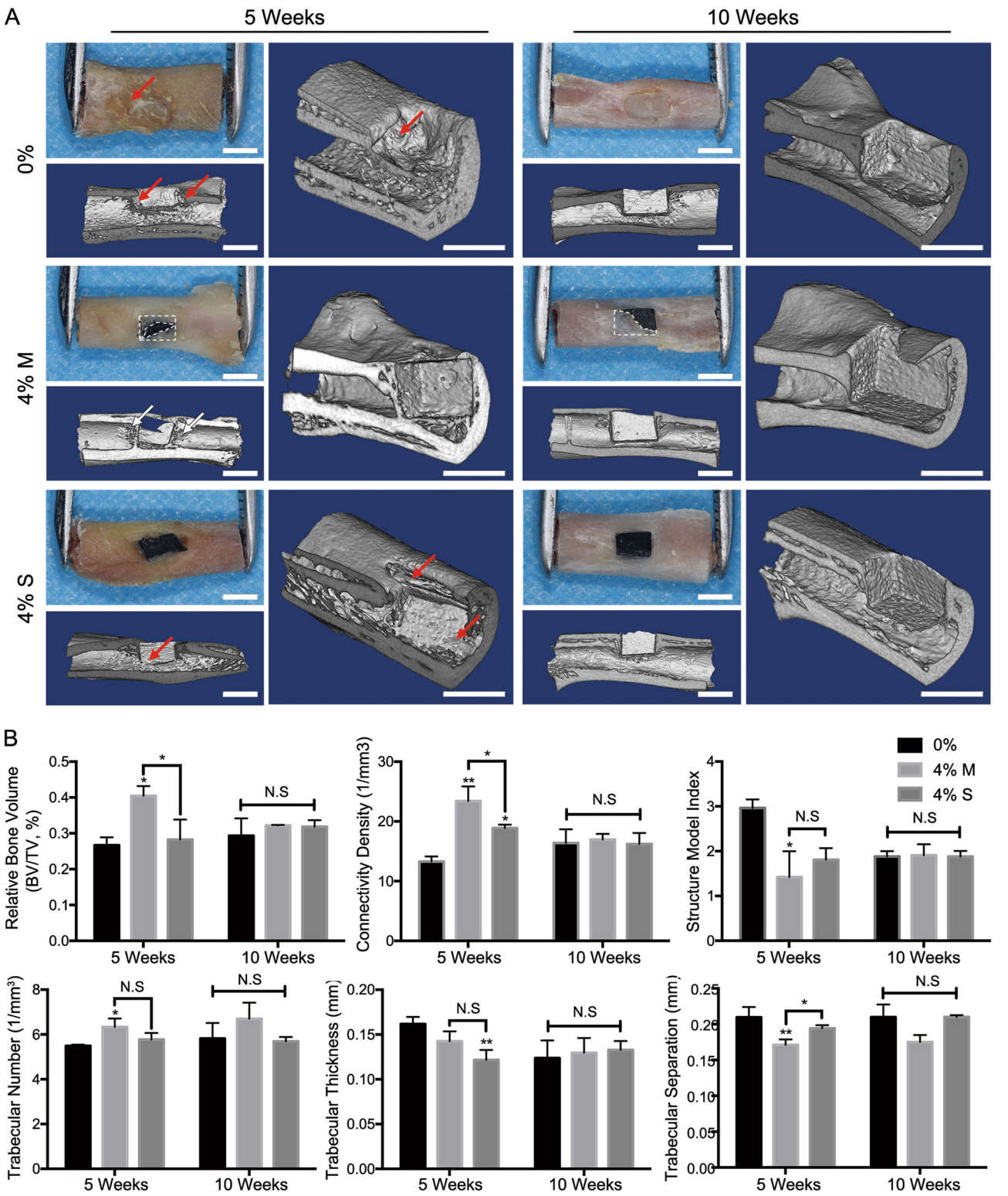

osteoinductivity in vivo when compared with pure PHBV and SWCNTs/PHBV composites (Fig. 5C). However, when the observation time was prolonged to 10 weeks, the expression of RUNX-2 showed no significant difference between pure PHBV and other composites.

4 Discussion

Considering the shortcomings of PHBV, several improvements have been reported, including direct modification of PHBV [28–30] and blending modifications with

◀ **Fig. 4** MWCNTs/PHBV composite stimulated more new bone and trabecula after implantation into rat femur. **a** Photograph and 3D reconstruction of femur segment at different time points after implantation ($n = 5$). New bone covering the composite represented by white dashed area; continuous new bone formation around composites represented by white arrow with black outline; connective tissue and region without new bone formation represented by red arrow. **b** Quantitative analysis of relative bone volume and trabecular morphology at different time points after implantation ($n = 5$). All parameters were calculated according to the region of interest (ROI), which was defined as around the composites near newly formed bone. Structure model index: 0-3; 0 for parallel plates, 3 for cylindrical rods. $^{*}P < 0.05$; $^{**}P < 0.01$; N.S not significant. Scale bar: 3 mm. All testing was replicated three times

hydroxyapatite (HA) [31], bioactive glass [32] and chitosan [33]. In this study, CNTs were used to strengthen the properties of PHBV.

The complete dispersion of CNTs should be achieved during the fabrication of composites since CNTs are likely to form agglomerations. It has been reported that the friction between CNTs within agglomeration greatly contributed to energy dissipation under heavy strain [34]. In addition, PHBV defects caused by agglomeration of CNTs might cause localized stress concentration, thus weakening the intensity of the composites. According to our SEM results, the complete dispersion of CNTs was achieved by ultrasound treatment. Similar to our previous study [27], agglomeration was observed when wt% of CNTs was increased, which might contribute to the observed decrease of flexural strength. It was also reported that randomly oriented CNTs reinforced the damping properties of the polymer composite [34], which was also achieved after ultrasonic dispersion. In summary, the characterization of the composites identified no significant difference between MWCNTs and SWCNTs. According to the result of XRD, the same patterns of PHBV crystallization were observed along with the addition of SWCNTs and MWCNTs, namely an increase in crystallinity and crystallite size. Similar results were reported by Shan G et al. [35], which demonstrated that CNTs acted as an effective heterogeneous nucleation agent and changed the crystallization behavior of PHBV. Furthermore, XRD results indicated that SWCNTs and MWCNTs have a similar effect on the crystallization of PHBV, which could explain why both SWCNTs and MWCNTs strengthen the composites.

The biocompatibility of nanocomposites based on PHBV has been reported previously [17, 19, 21]. However, no research has been published about the fabrication of composite of PHBV/SWCNTs, let alone a comparison between MWCNTs and SWCNTs in PHBV-based composites. In this study, primary cranial rOBs were cultured and seeded onto the composites. According to the absorbance obtained by CCK-8 test, the viability of cells seeded on pure PHBV and composites was inhibited at different time points when compared to direct seeding on a culture plate. With prolonged culture, cell viability recovered. Since the mechanism of CCK-8 test is based on water-soluble formazan dye generated by dehydrogenases [36], it can only reflect the numbers of living cells, rather than distinguish the inhibition of cell proliferation from cell death. Thus, PI was used to mark dead cells and flow cytometry was performed to determine the percentage of dead cells. Interestingly, only 12% of cells were identified as dead cells in the pure PHBV group, while the inhibition rate detected by CCK-8 was around 40%. As seen on our histogram, the addition of CNTs decreased the percentage of dead cells. Furthermore, MWCNTs/PHBV composites showed a smaller proportion of dead cells with no difference in cell viability when comparing pure PHBV and SWCNTs/PHBV composites.

The results of CCK-8 and flow cytometry indicated that PHBV caused a combination of cell proliferation inhibition and cell death. Importantly, the addition of CNTs to composites decreased the cell death caused by PHBV, without apparent effect on cell proliferation. The safety of PHBV depends on its residual monomers, namely hydroxybutyrate and hydroxyvalerate. Low molecular-weight PHB are naturally distributed in the cytoplasm and intracellular fluid, existing as PHB-protein complex [37] or PHB-Ca^{2+}-polyphosphate complex [38]. In addition, D-3- hydroxybutyrate, a degradation product of PHBV, is a natural component of human blood [39]. Our literature of CNTs/PHAs family composite literature revealed that Misra S et al. [26] reported the fabrication of poly (3-hydroxybutyrate) composites with bioactive glass particles and MWCNTs, and determined the formation of hydroxyapatite layer on PHBV/MWCNTs composites (without bioglass) after a 2-month immersion in simulated body fluid (SBF). The culturing of an osteoblast-like cell line on PHBV/MWCNTs composite was also reported, and a similar pattern of cell proliferation inhibition and decreased cell death was observed on these composites [25].

In our previous work [27], rat bone marrow stem cells were cultured on MWCNTs/PHBV composites to determine the biocompatibility, while the differentiation of stem cells was not detected. To further investigate the osteoinductivity of composites, as well as to compare MWCNTs and SWCNTs, total RNA was extracted to detect the transcriptional level of osteogenesis-related genes. Several genes expressed at different stage of osteogenesis was selected, and the expression level of all genes was upregulated mainly at day 1 and day 7 after seeding. Interestingly, the early and middle stage of osteogenesis-related genes, namely *Runx-2* and *Bmp-2* increased significantly in 4 wt% SWCNTs/PHBV composites one day after seeding, while late-stage genes, like *Opn* and *Ocn*, were upregulated more by 4 wt% MWCNTs/PHBV composites at day 7 after seeding. Taken together, these results indicated that the

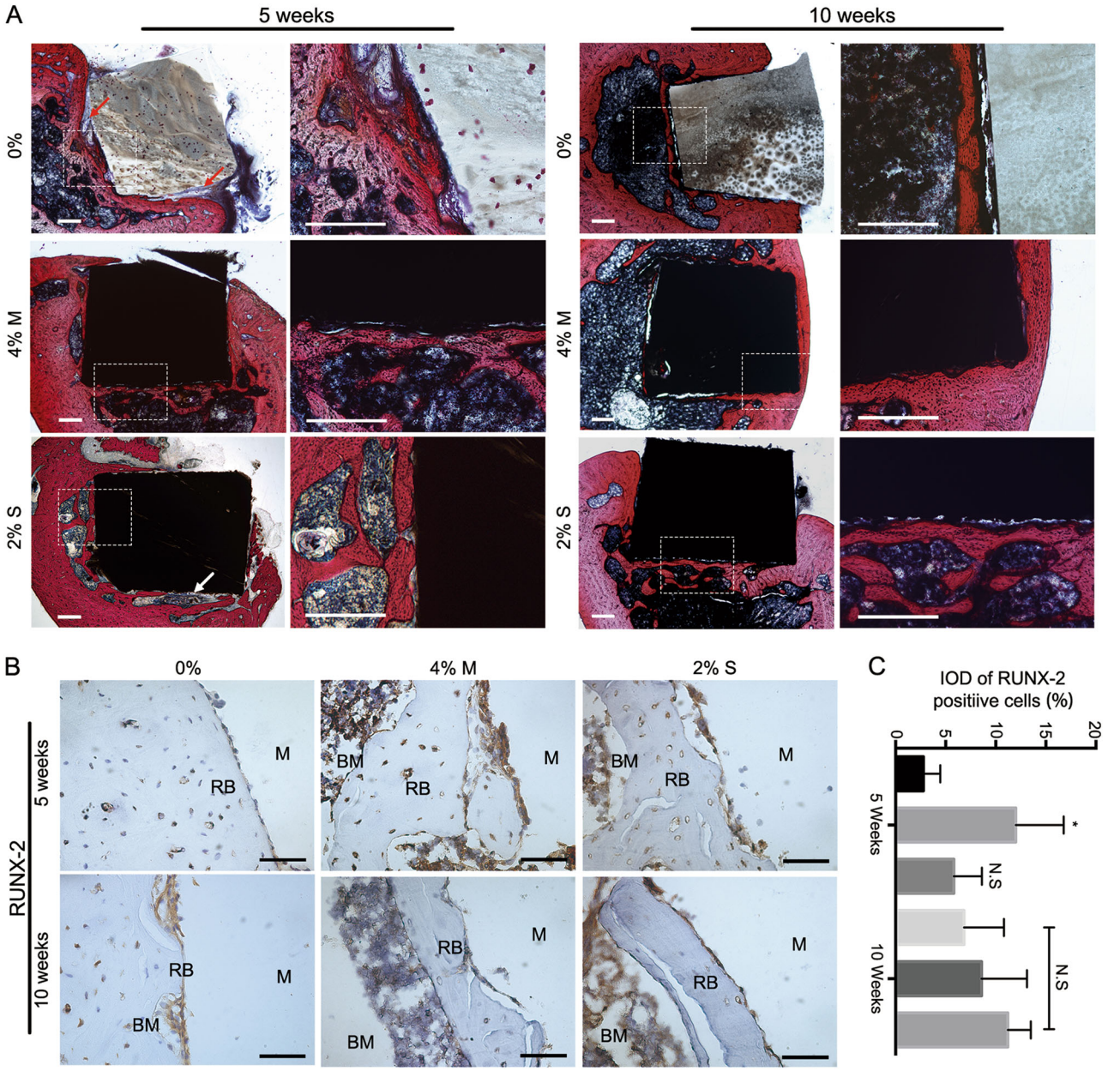

Fig. 5 MWCNTs/PHBV composite was more closely connected with new bone and upregulation of osteogenic-related genes. **a** Hard tissue slices from different treatment groups at different time points after implantation. Connective tissue and region without new bone formation represented by red arrows; zooming area represented by white dashed area. **b** IHC staining of RUNX-2 positive cells in newly regenerated bone and tissue around composites at different time points after implantation. RB: regenerated bone; BM: bone marrow; M: material. **c** Quantification of RUNX-2 expression as observed by integral optical density (IOD) of the positive area ($n = 5$). $^{*}P < 0.05$; N.S not significant. Scale bar: 500 μm. All testing was replicated three times

composites simultaneously inhibit the cell proliferation and upregulate the expression of functional osteoblast genes, which is similar to the behavior of stem cells in the process of differentiation.

According to these in vitro results, CNTs/PHBV composites showed a potential of application in bone tissue engineering. Since bone tissue engineering material must co-exist with host cells long-term, which is not easy to stimulate in vitro, we constructed a rat femoral bone defect to observe the interface reaction preliminarily between composites and host cells. Five weeks after implantation, new bone formation was observed around both pure PHBV and the composites. This new bone was intact and formed a close connection to MWCNTs/PHBV composites when compared with pure PHBV and SWCNTs/PHBV composites. The composites were covered, and even entirely

wrapped by the new bone in MWCNTs group. In addition, analysis of trabecular morphology showed an increased amount, thickness and mutual connection of newly formed trabecula in MWCNTs group when compared with PHBV and SWCNTs group. Importantly, a layer of periosteum-like tissue was observed at the interface between material and regenerated bone, which was composed of cells with strong expression of RUNX-2, especially in MWCNTs/PHBV group, which is consistent with the in vitro results. In summary, the biocompatibility and osteoinductivity of CNTs/PHBV composites were proved in vivo and in vitro.

The mechanism by which osteogenesis is induced by MWCNTs/PHBV composites has not been fully elucidated. Fukada E and Ando Y [40] reported that PHB and PHBV possess piezoelectric properties, and it has been reported that PHB-based composites induced osteogenesis due to their piezoelectric properties [41]. On the other hand, it was reported that CNTs were able to activate ß1-integrin signaling [42], which was recently found to mediate the BMP-2 dependent osteoblast differentiation and osteogenesis [43]. However, the mechanism underlying the difference between MWCNTs and SWCNTs was still unclear. It is possible that since the outer diameter of MWCNTs is 10–30 times larger than SWCNTs, more carboxyl functional group might exist on the surface of composites, which might affect the adhesion and differentiation of rOBs. It was also reported that SWCNTs caused more apparent cytotoxicity when compared with MWCNTs on macrophages [44], fibroblasts [45], and monocytes [46], which could explain the better biocompatibility of MWCNTs/PHBV composites.

Cytotoxicity is a major obstacle to the application of CNTs in tissue engineering. CNTs tend to clump together and form entangled structures and small aggregations. The mechanism of cytotoxicity of CNTs is very similar to asbestos, a classical pathogenic fibers [47]. It has been found that CNTs could induce oxidative stress, increasing the production of reactive oxygen species (ROS) [48, 49]. Elevated ROS production can activate specific transcription factors related to inflammation (such as NF-κB) [50], while low production of ROS will result in cell survival by activation of Nrf2 [51]. The following factors were reported to contribute to the toxicity of CNTs: fewer number of walls (SWCNTs), length (>15 μm), the formation of aggregation and lack of surface modification [51]. In our study, carboxyl group functionalized CNTs were used. According to SEM imaging, after complete ultrasonic dispersion, few aggregations were found at proper %wt of CNTs in composites. Furthermore, only the tail end of CNTs (0.1–1 μm) is exposed on the surface of the composites, which is much shorter than the length that would induce cytotoxicity. Coupled with the superiority of MWCNTs over SWCNTs, the biocompatibility of MWCNTs/PHBV composite was found to be superior in this study.

Through fabrication of MWCNTs/PHBV composites, we achieved improvement of PHBV material mechanical properties, thermostability, biocompatibility, and osteoinductivity both in vitro and in vivo. Importantly, the flexural strength of composites was elevated to the proximate level of bone cortex [52]. With the increase in thermal decomposition temperature, it was more convenient to shape composites using the thermoplastic properties of PHBV. The exact mechanism of action of osteoinductivity of MWCNTs/PHBV composites requires further investigation, and proper methods of fabricating biodegradable porous composites should also be elucidated.

5 Conclusion

CNTs/PHBV composites were fabricated by ultrasonic dispersion of MWCNTs and SWCNTs in PHBV, and were then shaped by thermal injection modeling. According to the SEM image, the complete dispersion of CNTs could be achieved when the wt% of CNTs was less than 4% in the composites. However, no difference in mechanical properties and thermostability was found between MWCNTs and SWCNTs. Primary rOBs were cultured with composites, with resulting cell proliferation inhibition observed by CCK-8. The most apparent cellular inhibition was detected 3 days after seeding uniformly among all groups, with cell growth recovery after 7 days. Cell death were observed by flow cytometry in PHBV group, which could be alleviated by the addition of CNTs, especially with 4 wt% of MWCNTs. Osteogenesis-related genes were upregulated both by PHBV and composites. Among which, SWCNTs/PHBV showed a more apparent effect on the early stage (1d), and MWCNTs/PHBV on the late stage (7d). Implantation of PHBV and composites was also performed in the femoral bone defect of SD rats. New bone formation was observed around the PHBV and composites. Similar to our in vitro results, in the MWCNTs/PHBV group, more newly formed trabecula, with closer integration to new bone, and earlier completed bone remodelling as well as higher expression of RUNX-2 were observed. Taken together, MWCNTs/PHBV composites showed better biocompatibility and osteoinductivity both in vitro and in vivo.

Acknowledgements This work was supported by the National Natural Science Foundation of China [grant numbers 81570987 and 81601909]; the Sichuan provincial science and Technology Foundation [grant number 2016FZ0074, 2017FZ0049 and 2016JY0142]; the Sichuan University Foundation for Young Teacher [2016SCU11053]. The funders did not participate in the design or undertaking of this study and preparation of the manuscript. We appreciate Dr. Chen L. from Analytical & Testing Center at Sichuan University for her generous help in MicroCT scanning 3D reconstruction of the samples. We are also grateful for the assistance of Dr. Zhang C. from the State Key Laboratory of Oral Diseases in SEM scanning.

Compliance with ethical standards

Conflict of interest The authors declare that they have no conflict of interest.

References

1. Mergaert J, Anderson C, Wouters A, Swings J, Kersters K. Biodegradation of polyhydroxyalkanoates. FEMS Microbiol Rev. 1992;9:317–21.
2. Byrom D. Production of poly-β-hydroxybutyrate: poly-β-hydroxyvalerate copolymers. FEMS Microbiol Lett. 1992;103:247–50.
3. Gogolewski S, Jovanovic M, Perren S, Dillon J, Hughes M. Tissue response and in vivo degradation of selected polyhydroxyacids: polylactides (PLA), poly(3-hydroxybutyrate) (PHB), and poly(3-hydroxybutyrate-co-3-hydroxyvalerate) (PHB/VA). J Biomed Mater Res. 1993;27:1135–48.
4. Kumarasuriyar A, Jackson R, Grondahl L, Trau M, Nurcombe V, Cool S. Poly(beta-hydroxybutyrate-co-beta-hydroxyvalerate) supports in vitro osteogenesis. Tissue Eng. 2005;11:1281–95.
5. Deepthi S, Nivedhitha Sundaram M, Vijayan P, Nair S, Jayakumar R. Engineering poly(hydroxy butyrate-co-hydroxy valerate) based vascular scaffolds to mimic native artery. Int J Biol Macromol. 2018;109:85–98.
6. Goonoo N, Khanbabaee B, Steuber M, Bhaw-Luximon A, Jonas U, Pietsch U, et al. kappa-Carrageenan enhances the biomineralization and osteogenic differentiation of electrospun polyhydroxybutyrate and polyhydroxybutyrate valerate fibers. Biomacromolecules. 2017;18:1563–73.
7. Gorodzha S, Muslimov A, Syromotina D, Timin A, Tcvetkov N, Lepik K, et al. A comparison study between electrospun polycaprolactone and piezoelectric poly(3-hydroxybutyrate-co-3-hydroxyvalerate) scaffolds for bone tissue engineering. Colloids Surf B Biointerfaces. 2017;160:48–59.
8. Vardhan H, Mittal P, Adena SKR, Upadhyay M, Yadav SK, Mishra B. Process optimization and in vivo performance of docetaxel loaded PHBV-TPGS therapeutic vesicles: a synergistic approach. Int J Biol Macromol. 2018;108:729–43.
9. Guo S, Zhu X, Loh X. Controlling cell adhesion using layer-by-layer approaches for biomedical applications. Mater Sci Eng C Mater Biol Appl. 2017;70(Pt 2):1163–75.
10. Hazer D, Kılıçay E, Hazer B. Poly(3-hydroxyalkanoate)s: Diversification and biomedical applications: a state of the art review. Mater Sci Eng C Mater Biol Appl. 2012;32:637–47.
11. Daitx T, Carli L, Crespo J, Mauler R. Effects of the organic modification of different clay minerals and their application in biodegradable polymer nanocomposites of PHBV. Appl Clay Sci. 2015;115:157–64.
12. Iijima S. Helical microtubules of graphitic carbon. Nature. 1991;354:56–8.
13. Li QW, Li Y, Zhang XF, Chikkannanavar S, Zhao Y, Dangelewicz A, et al. Structure-dependent electrical properties of carbon nanotube fibers. Adv Mater. 2007;19:3358–63.
14. Pop E, Mann D, Wang Q, Goodson K, Dai H. Thermal conductance of an individual single-wall carbon nanotube above room temperature. Nano Lett. 2006;6:96–100.
15. Ruoff R, Lorents D. Mechanical and thermal properties of carbon nanotubes. Carbon N Y. 1995;33:925–30.
16. Yakobson B, Avouris P. Mechanical properties of carbon nanotubes. In: Dresselhaus M, Dresselhaus G, Avouris P, editors. Carbon nanotubes: synthesis, structure, properties, and applications. Heidelberg: Springer Berlin Heidelberg; 2001. p. 287-327.
17. Shi X, Sitharaman B, Pham QP, Liang F, Wu K, Edward Billups W, et al. Fabrication of porous ultra-short single-walled carbon nanotube nanocomposite scaffolds for bone tissue engineering. Biomaterials. 2007;28:4078–90.
18. Sitharaman B, Shi X, Walboomers XF, Liao H, Cuijpers V, Wilson LJ, et al. In vivo biocompatibility of ultra-short single-walled carbon nanotube/biodegradable polymer nanocomposites for bone tissue engineering. Bone. 2008;43:362–70.
19. Martinelli V, Cellot G, Toma F, Long C, Caldwell J, Zentilin L, et al. Carbon nanotubes promote growth and spontaneous electrical activity in cultured cardiac myocytes. Nano Lett. 2012;12:1831–8.
20. Stout DA, Basu B, Webster TJ. Poly(lactic-co-glycolic acid): carbon nanofiber composites for myocardial tissue engineering applications. Acta Biomater. 2011;7:3101–12.
21. Keefer E, Botterman B, Romero M, Rossi A, Gross G. Carbon nanotube coating improves neuronal recordings. Nat Nanotechnol. 2008;3:434–9.
22. Ilbasmis-Tamer S, Ciftci H, Turk M, Degim T, Tamer U. Multiwalled carbon nanotube-chitosan scaffold: cytotoxic, apoptoti c, and necrotic effects on chondrocyte cell lines. Curr Pharm Biotechnol. 2017;18:327–35.
23. Lee H, Sang Shin U, Lee J, Kim H. Biomedical nanocomposites of poly(lactic acid) and calcium phosphate hybridized with modified carbon nanotubes for hard tissue implants. J Biomed Mater Res B Appl Biomater. 2011;98:246–54.
24. Wang S, Li Y, Zhao R, Jin T, Zhang L, Li X. Chitosan surface modified electrospun poly(epsilon-caprolactone)/carbon nanotube composite fibers with enhanced mechanical, cell proliferation and antibacterial properties. Int J Biol Macromol. 2017;104:708–15. (Pt A)
25. Misra S, Ohashi F, Valappil S, Knowles J, Roy I, Silva S, et al. Characterization of carbon nanotube (MWCNT) containing P (3HB)/bioactive glass composites for tissue engineering applications. Acta Biomater. 2010;6:735–42.
26. Misra S, Watts P, Valappil S, Silva S, Roy I, Boccaccini A. Poly (3-hydroxybutyrate)/Bioglass (R) composite films containing carbon nanotubes. Nanotechnology. 2007;18:075701.
27. Li J, Yang Z, Loo W, Xiao X, Zhang D, Cheung M, et al. In vitro and in vivo biocompatibility of multi-walled carbon nanotube/biodegradable polymer nanocomposite for bone defects repair. J Bioact Compat Polym. 2014;29:350–67.
28. Iwata T. Strong fibers and films of microbial polyesters. Macromol Biosci. 2005;5:689–701.
29. Tanaka T, Fujita M, Takeuchi A, Suzuki Y, Uesugi K, Ito K, et al. Formation of highly ordered structure in poly[(R)-3-hydroxybutyrate-co-(R)-3-hydroxyvalerate] high-strength fibers.Macromolecules. 2006;39:2940–6.
30. Wang W, Zhang Y, Zhu M, Chen Y. Effect of graft modification with poly (N-vinylpyrrolidone) on thermal and mechanical properties of poly (3-hydroxybutyrate-co-3-hydroxyvalerate). J Appl Polym Sci. 2008;109:1699–707.
31. Sultana N, Khan TH. In vitro degradation of PHBV scaffolds and nHA/PHBV composite scaffolds containing hydroxyapatite nanoparticles for bone tissue engineering. J Nanomater. 2012;2012:1–12.
32. Li H, Du R, Chang J. Fabrication, characterization, and in vitro degradation of composite scaffolds based on PHBV and bioactive glass. J Biomater Appl. 2005;20:137–55.
33. Zhang S, Prabhakaran M, Qin X, Ramakrishna S. Biocomposite scaffolds for bone regeneration: role of chitosan and hydroxyapatite within poly-3-hydroxybutyrate-co-3-hydroxyvalerate on mechanical properties and in vitro evaluation. J Mech Behav Biomed Mater. 2015;51:88–98.
34. Gardea F, Glaz B, Riddick J, Lagoudas D, Naraghi M. Identification of energy dissipation mechanisms in CNT-reinforced nanocomposites. Nanotechnology. 2016;27:105707.

35. Shan G, Gong X, Chen W, Chen L, Zhu M. Effect of multi-walled carbon nanotubes on crystallization behavior of poly(3-hydroxybutyrate-co-3-hydroxyvalerate). Colloid Polym Sci. 2011;289:1005–14.
36. Tominaga H, Ishiyama M, Ohseto F, Sasamoto K, Hamamoto T, Suzuki K, et al. A water-soluble tetrazolium salt useful for colorimetric cell viability assay. Anal Commun. 1999;36:47–50.
37. Goonoo N, Bhaw-Luximon A, Passanha P, Esteves S, Jhurry D. Third generation poly(hydroxyacid) composite scaffolds for tissue engineering. J Biomed Mater Res B Appl Biomater. 2017;105:1667–84.
38. Reusch RN. Low molecular weight complexed poly(3-hydroxybutyrate): a dynamic and versatile molecule in vivo. Can J Microbiol. 1995;41:50. Suppl 1(13)
39. Grøndahl L, Chandler-Temple A, Trau M. Polymeric grafting of acrylic acid onto poly(3-hydroxybutyrate-co-3-hydroxyvalerate): surface functionalization for tissue engineering applications. Biomacromolecules. 2005;6:2197–203.
40. Fukada E, Ando Y. Piezoelectric properties of poly-β-hydroxybutyrate and copolymers of β-hydroxybutyrate and β-hydroxyvalerate. Int J Biol Macromol. 1986;8:361–6.
41. Doyle C, Tanner E, Bonfield W. In vitro and in vivo evaluation of polyhydroxybutyrate and of polyhydroxybutyrate reinforced with hydroxyapatite. Biomaterials. 1991;12:841–7.
42. Sun H, Lü S, Jiang X, Li X, Li H, Lin Q, et al. Carbon nanotubes enhance intercalated disc assembly in cardiac myocytes via the β1-integrin-mediated signaling pathway. Biomaterials. 2015;55:84–95.
43. Brunner M, Mandier N, Gautier T, Chevalier G, Ribba A, Guardiola P, et al. β1 integrins mediate the BMP2 dependent transcriptional control of osteoblast differentiation and osteogenesis. PLoS One. 2018;13:e0196021.
44. Jia G, Wang H, Yan L, Wang X, Pei R, Yan T, et al. Cytotoxicity of carbon nanomaterials: single-wall nanotube, multi-wall nanotube, and fullerene. Environ Sci Technol. 2005;39:1378–83.
45. Tian F, Cui D, Schwarz H, Estrada GG, Kobayashi H. Cytotoxicity of single-wall carbon nanotubes on human fibroblasts. Toxicol Vitr. 2006;20:1202–12.
46. Inoue K, Takano H, Koike E, Yanagisawa R, Sakurai M, Tasaka S, et al. Effects of pulmonary exposure to carbon nanotubes on lung and systemic inflammation with coagulatory disturbance induced by lipopolysaccharide in mice. Exp Biol Med. 2008;233:1583.
47. Brown D, Beswick P, Donaldson K. Induction of nuclear translocation of NF-kappaB in epithelial cells by respirable mineral fibres. J Pathol. 1999;189:258–64.
48. Li Z, Hulderman T, Salmen R, Chapman R, Leonard S, Young S, et al. Cardiovascular effects of pulmonary exposure to single-wall carbon nanotubes. Environ Health Perspect. 2007;115:377–82.
49. Shvedova A, Kisin E, Mercer R, Murray A, Johnson V, Potapovich A, et al. Unusual inflammatory and fibrogenic pulmonary responses to single-walled carbon nanotubes in mice. Am J Physiol Lung Cell Mol Physiol. 2005;289:L698–708.
50. Manna S, Sarkar S, Barr J, Wise K, Barrera E, Jejelowo O, et al. Single-walled carbon nanotube induces oxidative stress and activates nuclear transcription factor-kappaB in human keratinocytes. Nano Lett. 2005;5:1676–84.
51. Johnston H, Hutchison G, Christensen F, Peters S, Hankin S, Aschberger K, et al. A critical review of the biological mechanisms underlying the in vivo and in vitro toxicity of carbon nanotubes: the contribution of physico-chemical characteristics. Nanotoxicology . 2010;4:207–46.
52. Velasco MA, Narvaez-Tovar CA, Garzon-Alvarado DA. Design, materials, and mechanobiology of biodegradable scaffolds for bone tissue engineering. Biomed Res Int. 2015;2015:729076.